Unraveling intrinsic correlation effects with angle-resolved photoemission spectroscopy

Jianqiang Sky Zhou, Lucia Reining, Alessandro Nicolaou, Azzedine Bendounan, Kari Ruotsalainen, Marco Vanzini, J. Kas, J. Rehr, Matthias Muntwiler, Vladimir Strocov, et al.

Unraveling intrinsic correlation effects with angle-resolved photoemission spectroscopy

Jianqiang Sky Zhou[a,b,c], **Lucia Reining**[a,b,1], **Alessandro Nicolaou**[d], **Azzedine Bendounan**[d], **Kari Ruotsalainen**[d], **Marco Vanzini**[a,b,e], **J. J. Kas**[f], **J. J. Rehr**[f], **Matthias Muntwiler**[g], **Vladimir N. Strocov**[g], **Fausto Sirotti**[h,1], **and Matteo Gatti**[a,b,d,1]

[a]Laboratoire des Solides Irradiés, École Polytechnique, CNRS, CEA/DRF/IRAMIS, Institut Polytechnique de Paris, F-91128 Palaiseau, France; [b]European Theoretical Spectroscopy Facility (ETSF); [c]Sorbonne Universitè, CNRS, Institut des Nanosciences de Paris, UMR7588, F-75252, Paris, France; [d]Synchrotron SOLEIL, L'Orme des Merisiers, Saint-Aubin, BP 48, F-91192 Gif-sur-Yvette, France; [e]Theory and Simulation of Materials (THEOS), École Polytechnique Fédérale de Lausanne, CH-1015 Lausanne, Switzerland; [f]Department of Physics, University of Washington, Seattle, Washington 98195-1560, USA; [g]Swiss Light Source, Paul Scherrer Institut, CH-5232 Villigen PSI, Switzerland; [h]Laboratoire de Physique de la Matière Condensée, CNRS, École Polytechnique, Institut Polytechnique de Paris, F-91128 Palaiseau, France

This manuscript was compiled on October 9, 2021

Interaction effects can change materials properties in intriguing ways, and they have in general a huge impact on electronic spectra. In particular, satellites in photoemission spectra are pure many-body effects, and their study is of increasing interest in both experiment and theory. However, the intrinsic spectral function is only a part of a measured spectrum, and it is notoriously difficult to extract this information, even for simple metals. Our joint experimental and theoretical study of the prototypical simple metal aluminum demonstrates how intrinsic satellite spectra can be extracted from measured data using angular resolution in photoemission. A novel kind of non-dispersing satellite is detected, which is due to electron-electron interactions and the thermal motion of the atoms. Additional non-dispersing intensity comes from the inelastic scattering of the outgoing photoelectron. The intrinsic spectral function, instead, has satellites that disperse both in energy and in shape. Theory and the information extracted from experiment describe these features with very good agreement.

ARPES | Plasmon satellites | First principles calculations

Photoemission spectroscopy is one of the most direct experimental tools to access band structures and excitation spectra of materials (1). Although the Coulomb interaction between electrons leads to a renormalization of energies and to lifetime broadening, the resulting quasiparticle (QP) band structure can usually still be detected, and, moreover, reproduced and interpreted using first-principles theoretical approaches (2, 3). However, the QPs constitute only part of the measured spectra. They are usually accompanied by an incoherent background and a series of additional structures called satellites, over a binding-energy range of several tens of eV. The satellite part of the spectra is in general much less studied than the QPs, although it is intriguing: whereas QPs can be understood qualitatively in a non-interacting picture, satellites are pure many-body effects (2). They cannot, by definition, be interpreted from a single-particle point of view. Therefore, they carry information complementary to the insight gained from the band structure.

To access this information, however, is difficult, and to quantify correlation effects from experiment alone, most often impossible. This holds true even for the simplest cases, such as plasmon satellites in simple metals, because intrinsic spectral functions are buried under strong additional contributions in the experiment. Theory and first principles calculations can give additional insight and indeed, the existence of satellite series is understood in terms of one or more bosonic excitations when an electron is removed from the sample (4–6). When the bosons are due to electronic excitations, this is translated into first principles calculations in the so-called GW+cumulant (GW+C) approach, where the screened Coulomb interaction W reflects the excitations (7); phonons can be treated in a similar way (8–10). The approach is increasingly popular, with an extension from the original core level spectroscopy applications (1, 4–6, 11) to valence bands (12–23), where completely new questions linked to the dispersion of bands and satellites appear. Like for the core levels, the existence and energies of the satellites are explained by GW+C also in the valence band, but the satellite intensity is not: in general, calculated satellites are much weaker than measured ones. This is a major drawback: while the energy carries precious information about the nature of the boson, the intensity is a measure of the correlation strength.

In this work, we show that *angle-resolved* photoemission spectroscopy (ARPES) can be used to overcome this difficulty. In the simplest view on dispersion, one would expect excitations at each point in the Brillouin zone to be approximately independent (14); in that case experiment and GW+C calculations should find plasmon or phonon replicas that disperse in energy following the QP bands. These replicas were indeed observed both in theory and angle-resolved experiment (16–19), but no quantitative comparison could be made. The main reason is the fact that first-principles calculations determine

Significance Statement

Photoemission spectra reflect the many-body electronic structure of materials. The main peaks whose energies vary as function of angle-resolved momentum usually correspond to the band structure. Replica of these peaks, called satellites, are entirely due to interactions. Therefore, they could be used to detect the strength of electronic correlation in a material, if intrinsic features were not buried by other scattering effects. This study demonstrates how intrinsic satellites can be unraveled from measured spectra using angular resolution and insights on the origin of non-dispersing satellite contributions. Consequently angle-resolved photoemission can be used to set an unambiguous lower bound on the strength of correlation.

M.G., L.R., F.S., V.S. and J.S.Z. designed the project; A.B., M.M., A.N., K.R., F.S., M.V. and J.S.Z. performed experiments; M.G., J.J.K., J.J.R and J.S.Z. performed calculations; all authors discussed the results, and M.G., L.R., F.S., and J.S.Z. wrote the paper with contributions from all authors.

The authors declare no competing interests.

[1]To whom correspondence should be addressed. E-mail: lucia.reining@polytechnique.edu, fausto.sirotti@polytechnique.edu, matteo.gatti@polytechnique.edu.

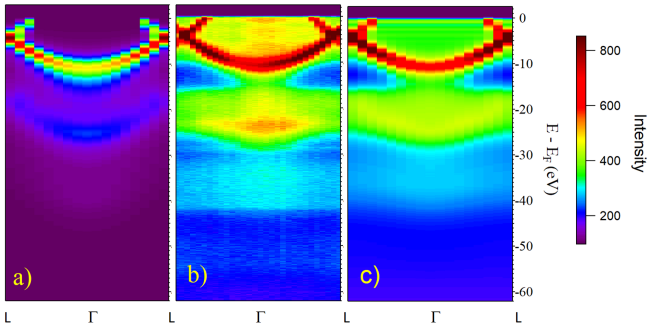

Fig. 1. (a) and (c) Calculated spectral functions and (b) experimental ARPES image in the ΓL direction. The results of *ab initio* GW+C calculations are (a) without and (c) with the Debye-Waller contribution and extrinsic and interference effects.

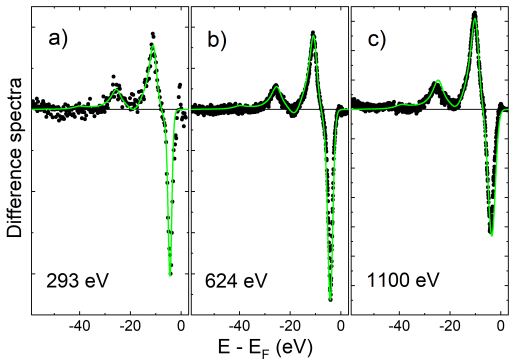

Fig. 2. Differences between spectra at the Γ and L points, at 293, 624 and 1100 eV photon energies: experimental results (black dots) are compared with calculations of intrinsic spectral functions (green lines).

the *intrinsic* spectral function *stemming from the valence band in a perfectly ordered crystal*, while this is only a small part of the experimental spectrum. In the following, we propose a way to extract this information from the measured data, and we explain effects that were not noticed previously, both in the intrinsic dispersing spectral function and in the total measured spectra.

Results

Overview. The experimental ARPES image obtained at 624 eV photon energy is shown in Fig. 1(b). One can clearly see the parabolic valence band of aluminum and its replica at a shift of about 15 eV. This shift is consistent with the bulk plasmon energy of aluminum (24). The GW+C intrinsic theoretical spectra, shown in Fig. 1(a), are in qualitative agreement with experiment concerning the valence bands and the presence of a dispersing satellite, similar to previous observations for silicon (16–18). Moreover, the existence of higher-order satellite replicas is confirmed, as expected from GW+C. Still, the comparison of theoretical and experimental panels shows large differences, of the order of the spectra themselves. An attempt to explain the valence spectra of aluminum was also made in (12, 13), by comparing results of GW+C calculations and electron momentum spectroscopy, but this did not give access to angle-resolved spectra, and significant discrepancies remained. In the present work, we include corrections due to inelastic scattering and temperature, leading to the final theoretical results in Fig. 1(c), in very good agreement with experimental spectra in Fig. 1(b).

The ideal intrinsic spectral function. Let us start with the crucial question: *Is it possible to infer information about the intrinsic spectral function from the experiment?* The most important contributions beyond the ideal intrinsic spectral function should be due to inelastic scattering of the outgoing photoelectron, temperature effects, and disorder. In all those cases, the photoelectron should lose its angular resolution. This would mean that even if the ideal intrinsic spectral function is only a small part of the spectra, it should dominate the *variation* of the spectra throughout the Brillouin zone.

To test this hypothesis, we take the difference between spectra measured at different angles and we consider the most different spectral functions, which are observed at Γ and L, after subtracting a Shirley background. The resulting difference

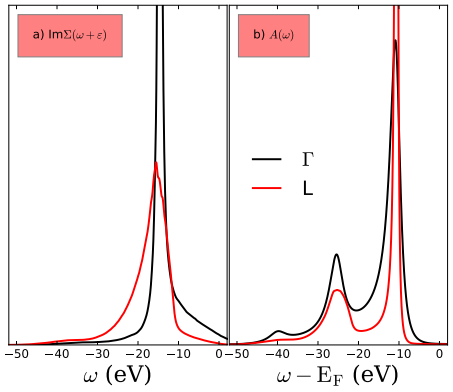

Fig. 3. (a) $\mathrm{Im}\Sigma^{\ell\ell}_{xc}(\omega+\varepsilon_\ell)$ at Γ (black) and L (red), (b) The corresponding intrinsic spectral function $A_\ell(\omega)$ at Γ and L. The QPs at Γ and L are aligned.

spectra are shown in Fig. 2 for photon energies of 293, 624 and 1100 eV. The negative feature close to the Fermi energy is due to the QP peak at L, and the following positive one is the QP at Γ. A clear satellite difference structure is found between −15 eV and −30 eV. All experimental features are perfectly well represented by the calculated difference of intrinsic spectral functions. This shows that the GW+C approach captures the many-body effects leading to the ideal intrinsic valence band satellites in a quantitative, very precise, way. Most importantly, it unambiguously supports our idea to use angle resolution in order to extract intrinsic information from the experiment.

On top of the dispersion in energy, the satellites also show a strong shape dispersion. In Fig. 3(b) the calculated spectral functions at Γ and L are compared by aligning the QP. In particular, whereas the QP is much sharper at L than at Γ due to lifetime broadening, the first intrinsic satellite is strong and sharp at Γ, and much more washed out at L; note that the satellite contribution at Γ looks more important at first sight, because the lifetime broadening of the QP contributes weight in the same energy region.

The fact that the satellite shape does not follow the QP shape may seem surprising. It is a feature that is intimately linked to the dispersion of the valence band: the imaginary part of the self-energy, which determines the satellites, is dominated

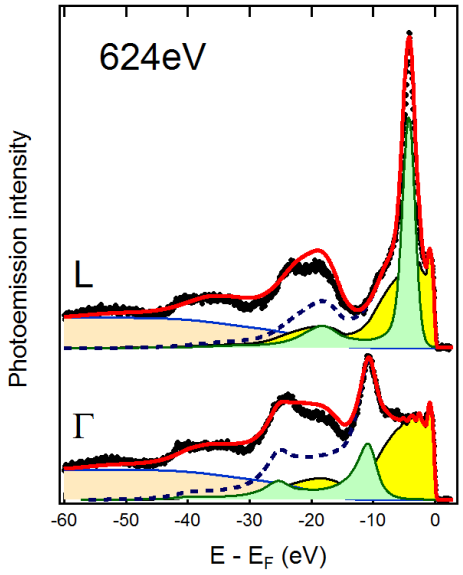

Fig. 4. The spectra at 624 eV photon energy at Γ and L. The Fermi energy is set to zero. Light green area is the ideal (i.e., zero-temperature) intrinsic angle-resolved spectral function $A^{int}_{\mathbf{k}}(\omega)$, yellow area is the angle-integrated $D^{int}(\omega)$ weighted by the Debye-Waller coefficient. Their sum is the black dashed curve and corresponds to the total intrinsic spectral function. The light brown area is a Shirley background derived from the integral of extrinsic and interference spectral intensities. The total theoretical spectrum (red line) is the sum of the total intrinsic spectral function, the background, and extrinsic and interference effects as predicted by a calculation based on the parameter-free model (26). It compares very well to the ARPES data (black dots).

by the excitation of the QP plus one or more bosons, but even for moderate coupling strength it also contains other possible excitations. Therefore, the satellites are *not* simple replica of the valence bands. In a simple metal like Al, electrons are coupled with the valence plasmon, which has a parabolic dispersion as a function of its wavevector $\mathbf{q}$. In the coupling with a single core level, which is very localized and has no dispersion, the shape of the satellites is entirely governed by the plasmon dispersion: it produces an asymmetric lineshape for each satellite, in general with a tail to higher binding energies (1, 6). In the valence band region of aluminum electrons are delocalized, and they couple therefore mostly with plasmons with momentum $\mathbf{q}$ close to 0. Indeed, while the calculated plasmon dispersion in Al ranges from 15 eV at $\mathbf{q} \to 0$ to about 25 eV at $\mathbf{q} = 1.0$ Bohr^{-1} (see, e.g., figure 8 in Ref. (25)), the peaks of the imaginary part of the exchange-correlation self-energy $\mathrm{Im}\Sigma^{\ell\ell}_{xc}(\omega + \varepsilon_\ell)$ shown in Fig. 3(a) are centred around 15 eV. Still, there is broadening, because other close lying QP excitations mix in. This asymmetric broadening therefore depends on the energies of the QP excitations available in the neighborhood of the measured $\mathbf{k}$ point. Since the band is flat and upwards dispersing at Γ whereas it is steep and quite symmetric at L, this neighbourhood is different for the two $\mathbf{k}$ points, so the satellites are different. More generally, also close lying bands will contribute to this effect, and the characteristic shape of the valence band satellites, and its dispersion, is governed by the density of valence states. The equations for a more formal discussion can be found in the Methods section.

Non-dispersing satellites: a temperature effect. The excellent agreement of the difference spectra in Fig. 2 leaves no doubt that the intrinsic contribution of the ideal crystal to the spectral function is actually quite small. Even better than in the overview Fig. 1, this can be appreciated in Fig. 4, which compares experimental and calculated spectra at 624 eV photon energy, at the Γ and L points. The light green areas are theoretical intrinsic spectral functions, and black dots are measured spectra. While some of the experimental structures can be identified in the calculated spectra, in particular the QPs at Γ and L, and part of the satellite structures, others are completely absent in the calculation: for example, the shoulder that is measured on the first satellite around -20 eV. This qualitative disagreement suggests that more interesting features remain to be discovered. In a real experiment on a real sample, spectra may consist of numerous potential contributions. Here we choose to concentrate on the following question: *Given the quasiparticles, what satellite spectra are predicted by theory, how well does this prediction match experiment, and what does this tell us about the physics?* As we will see, even a simple metal like aluminum constitutes a rich playground.

In order to understand satellites, one has to start with the QP. In the QP region, the big difference between the measured spectra and the intrinsic spectral function is the important spectral weight close to the Fermi level that appears in the experimental spectrum taken at Γ, where aluminum should have no valence band intensity. The presence of such additional intensity in the QP band-structure region has been discussed as a consequence of Debye-Waller (DW) effects on photoemission matrix elements* (28–30): Even at temperatures as low as 50 K, in aluminum the disordered thermal vibrations of the atoms destroy the $\mathbf{k}$-selectivity of the ARPES, giving rise to a non-dispersive component in the spectrum, which amounts to integrating the different contributions from the $\mathbf{k}$-resolved spectra over the BZ (31). For increasing photon energy and temperature, the $\mathbf{k}$-integrated spectrum tends to become the dominant component, thus being one of the limiting factors for the angle resolution in hard x-ray photoemission spectroscopy experiments (32–34).

Since aluminum is a metal, the loss of $\mathbf{k}$-resolution explains the fact that even in our experimental spectrum at Γ, which is at the bottom of the band, much intensity is found at the Fermi level. Other possible explanations such as surface photoelectric effects (35, 36) and the k_z intrinsic broadening of the final state (37) were discarded here since they are not sufficient to reproduce this additional intensity. We can also exclude many-body effects neglected in GW+C, in particular electronic recoil, see e.g. Sec. 4.3 in (38). The neglect of recoil is more justified close to Γ, where the band is flat, than at L, where it is very steep. Instead we observe similar agreement with experiment at the two points. Moreover, the recoil approximation refers to the intrinsic spectral function, so there would be no explanation for the photon energy dependence. We therefore suppose that DW is the dominant mechanism.

In the simplest approximation, the $\mathbf{k}$-resolved and $\mathbf{k}$-integrated components are weighted by the Debye-Waller factors $\mathcal{W}$ and $1 - \mathcal{W}$, respectively. We determine $\mathcal{W}$ by fitting the spectra in the QP region, using the angle-resolved and Brillouin zone-integrated QPs of the calculated spectra (light

*Note that this is different from the electron-phonon interaction (27), which can affect the QP energy and produce satellites in the $\mathbf{k}$-resolved spectral function (9, 10), with binding energy smaller than the present experimental resolution.

green and yellow areas respectively). The QP spectra at Γ and L are very well reproduced by a single coefficient, $\mathcal{W} = 0.46$. This observation supports the assumption that temperature is the main responsible for the non-dispersing QP spectral weight. Moreover, according to (29) the Debye-Waller factor is approximately given by: $\mathcal{W} = \exp\left[-\frac{1}{3}\Delta k^2 \langle U^2(T)\rangle\right]$, where Δk is the momentum transfer at the photon energy of the measurement and $\langle U^2(T)\rangle$ is the three-dimensional mean-squared vibrational displacement, which can be estimated using the Debye temperature of the material and the temperature T of the sample. For bulk aluminum at 77 K, the model estimates $\mathcal{W} = 0.53$ which is consistent with our finding and gives additional support to our hypothesis. Finally, the fit of the QP is refined by adding two extra peaks with the shape of the QP at Γ, at 10.8 and 8 eV binding energy, respectively. Their weights are very small, and given for completeness in the Supplementary Information (SI).

While the importance of DW on the band-structure region is established (28–30), its effect on satellites, to the best of our knowledge, has not heretofore been investigated. The question is therefore whether, and in which way, the DW physics is also responsible for strong modifications of the satellites. It is reasonable to surmise that plasmon satellites are created in the same way in ordered and thermally disordered systems. This would suggest that the angle-integrated QP component due to the DW effect leads to angle-integrated satellites, in the same way as for the angle-resolved QPs and their satellites. If this hypothesis were true, one should be able to describe QPs and satellites with a similar DW approach. We therefore adopt the following procedure: We call $A^{int}_{\mathbf{k}}$ the calculated $\mathbf{k}$-resolved intrinsic spectral function, including its satellites, and $D^{int}(\omega)$ the corresponding $\mathbf{k}$-integrated spectrum.

The total intrinsic spectral function is then obtained as the weighted sum $\mathcal{W}A^{int}_{\mathbf{k}}(\omega) + (1-\mathcal{W})D^{int}(\omega)$. The result is the black dot-dashed curve in Fig. 4. One can now recognize all the main features of the experimental spectra, including the tendency to form a shoulder on the low–binding-energy side of the satellites. Clearly, the non-dispersing DW satellites give a very important contribution to the spectra, and they explain, at least qualitatively, the observed spectral shape.

Scattering contributions to the non-dispersing satellites. It should not be expected that the intrinsic spectral function compares quantitatively with experiment, since it does not include effects due to inelastic scattering of the outgoing photoelectron, called extrinsic and interference effects (39). The magnitude and consequences of these effects have been subject to vivid discussion; see, e.g. (1, 40–43). Usually they are neglected in first-principles calculations. Recently the model approach of Refs. (6, 26, 44) was combined with first-principles calculations of spectral functions to discuss angle-integrated spectra of silicon (14), and comparison with experiment was significantly improved with respect to a purely intrinsic calculation. In this approach, the enhancement of satellites due to inelastic scattering is derived from the semi-infinite homogeneous electron gas. However, it applies to angle-integrated spectra. Here, we extend this parameter-free approach to the case of ARPES.

The new difficulty is that both the angle-resolved and angle-integrated intrinsic $A^{int}_{\mathbf{k}}(\omega)$ and $D^{int}(\omega)$ require extrinsic and interference corrections, due to the scattering of the respective photoelectrons. However, one should expect that the inelastic scattering of the outgoing electrons from the angle-resolved electrons also leads to a loss of $\mathbf{k}$-resolution (44). This explains why difference spectra directly yield the *intrinsic* spectral functions. It means that it would not be correct to enhance the angle-resolved satellites in the same way as the angle-integrated contributions. Instead, we determine the satellite enhancement following the approach in (14), deduce from this the scattering contributions for each $\mathbf{k}$-point and integrate them over the Brillouin zone. Details are given in the Methods section and the SI.

Finally, there is a background of secondary processes that is proportional to the part of the spectrum due to inelastic scattering. To take this into account we add a Shirley background (light brown areas) created solely by the extrinsic/interference contributions, reflecting the fact that most of the scattering is already accounted for explicitly. The red curves in Fig. 4 and Fig 1(c) are our final result. The agreement with ARPES data is very good. Note that besides a single factor scaling the intensity of the secondary electron background, these results have been obtained without any free parameter in the description of the satellites.

Photon energy dependence. The photon energy dependence further supports our interpretation. We have taken spectra at 1100 eV and followed in detail the same procedure as for 624 eV. At higher photon energy the DW factor $\mathcal{W}$ should decrease, because the momentum transfer enters the negative exponent, as explained above. This is indeed the case: Fig. 5 shows results for a photon energy of 1100 eV. Our fit on the QP predicts a decrease of the Debye-Waller factor to a value of $\mathcal{W} = 0.395$. This is consistent with the DW model (29), which would yield a decrease to $\mathcal{W} = 0.33$ at T=77 K, whereas it rules out an important role of intrinsic disorder. It gives further strong evidence for our conjecture, where the intrinsic part of the dispersionless satellites consists of shape-modified replica of QPs with a loss of $\mathbf{k}$-resolution due to the DW effect, reflecting therefore directly the peaks in the density of valence states. Also the photon-energy dependent extrinsic and interference contributions are well described by our calculations, as can be seen from the very good agreement between experiment and the final theoretical results in Fig. 5.

Discussion

Altogether, our joint experimental and theoretical study yields an understanding of the photoemission spectra of aluminum well beyond the simple picture of bands and their plasmon replicas, suggesting how to overcome some major problems of the interpretation of photoemission data, and opening several interesting and general perspectives. First, there is a long standing gap between theory and experiment, with theory mostly focusing on the description of correlation effects in the intrinsic spectral function of the ideal crystal, which is only a fraction of the experimental result. We have shown how information concerning the ideal intrinsic spectral function (i.e. without thermal atomic vibrations, and without extrinsic scattering of the photoelectron, and interference effects) can be extracted from ARPES measurements, and we have found that there is excellent agreement between these experimental results and the calculated intrinsic spectral functions. Interestingly, the intrinsic satellites have a shape that is determined by the valence density of states, rather than by the plasmon

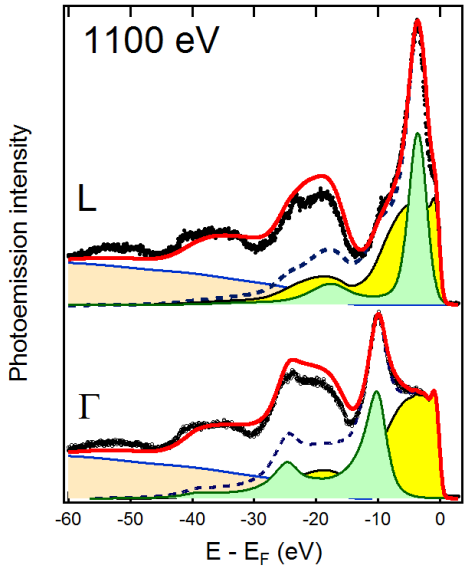

Fig. 5. The spectra at 1100 eV photon energy for the Γ and L points. The theoretical spectra (red lines) are obtained as in Fig. 4.

dispersion, which instead determines the shape of core level satellites. We have also shown that atomic thermal motion causes the appearance of dispersionless satellites, due to a loss of momentum conservation for both the QPs and their satellites. These dispersionless satellites can be pronounced in the valence spectra, corresponding to replicas of peaks in the density of states, and they should not be confused with signals due to impurities. They are reinforced by inelastic scattering of the outgoing photoelectrons, which lose momentum resolution and energy by exciting electron-hole pairs and plasmons. Once cross sections and surface effects are fitted on the quasiparticles, our calculations of the final spectra are parameter-free, besides a scaling factor for the remaining secondary electron background. For photon energies of 624 eV and 1100 eV, where measurements start to be bulk sensitive, they lead to very good agreement with experiment. This agreement and the observed trends fully confirm our conjectures. Since none of our calculations explicitly includes the real surface, the agreement should be much worse at lower photon energies, where the measurements are clearly surface sensitive. Interestingly, this does not hold for the dispersing part of the intrinsic spectral function that is still very well described, as can be seen in Fig. 2. This indicates that it is a bulk property that can be extracted from ARPES even at low photon energy. Instead, the thermal motion of atoms at the surface is larger than in the bulk, which leads to an enhancement of the DW effect (29). More generally, scattering appears to be much increased, well beyond the predictions based on the semi-infinite homogeneous electron gas (6, 26, 44). An illustration for 293 eV can be found in the SI.

Our results open several broad perspectives: in particular, aluminum exhibits a relatively strong DW effect, but it is not a singular case: many other metals or semiconductors, such as silicon, are equally good candidates for materials where this new kind of dispersionless satellites should be observable. Indeed, one may note, e.g., several sharp dispersionless features visible in the valence band QP region of the photoemission spectra of silicon (see Fig. 1(a) of (17)), at energies corresponding to peaks in the density of states of silicon. This suggests that a closer analysis of the data in the satellite region, for silicon and for other materials with a similarly strong DW effect, should indeed reveal their replica. The fact that valence band satellites disperse not only in energy, but also in shape, also merits further attention. This information is difficult to extract from classical overview spectra such as the one given in Fig. 1, whereas our work suggests how to simulate and analyze single spectra.

Most importantly, since we have shown that the intrinsic spectral properties may be isolated in the experiment by taking difference spectra, the analysis of the contributions linked to dispersing QPs allows one to isolate ideal intrinsic, temperature, and extrinsic/interference effects. This highlights the important role that ARPES measurements may play in order to unambiguously distinguish intrinsic correlation effects from other factors that dominate the experiments. The importance of a tight interplay of theory and experiment in order to obtain deeper understanding is particularly noteworthy to stress, and the procedure suggested here may be useful for many further investigations on other materials.

Materials and Methods

We have performed state-of-the-art ARPES measurements and first-principles GW+C calculations of aluminum (45), yielding the band structure and the first three dispersing satellites along the ΓL direction of the Brillouin zone. Data supporting this article are available from the authors upon reasonable request.

Experiment. ARPES experiments were performed at about 50 K using a Scienta EW4000 hemispherical electron analyzer at the PEARL beamline of the Swiss Light Source (46). The Al($\bar{1}$01) surface was prepared with several sputtering and annealing cycles until the observation of an oxygen contamination below 1% of a monolayer and a sharp low-energy electron diffraction pattern. The single-crystal sample contained about 0.02% atom concentration of Ta impurities. Because of their extremely high cross section, Ta $4f$ photoelectrons show up as a sharp doublet line in the spectrum at the characteristic binding energies of 21.7 and 23.57 eV. Two Gaussian peaks at these energies have thus been removed in the angle-resolved spectra. Raw data are shown in the SI.

Photon-energy dependent ARPES experiments were used to measure the Fermi surface periodicity in the surface-normal (k_z) direction and to identify the photon energies corresponding to the Γ points of 4 consecutive Brillouin zones. ARPES experiments on a 60 eV binding energy range were then performed at $h\nu$ = 293 eV, 624 eV and 1100 eV photon energies. These correspond to small deviations along the k_z-direction, which at Γ were evaluated respectively as: -0.1, 0.15 and 0.29 of ΓK (and similarly for the other points along ΓL). The energy and angular resolutions at 293 eV photon energy were 0.12 eV and 1/20 of ΓL, respectively; 0.18 eV and 1/14 of ΓL at 624 eV; and 0.45 eV and 1/10 of ΓL at 1100 eV. The spectra at $h\nu$ =293 eV are highly surface sensitive and are given in the SI for completeness. For quantitative comparison with theory, the experimental spectra have been corrected for the change of intensities throughout the Brillouin zone due to photoelectron diffraction (47, 48) by normalizing intensities of non-dispersing features. More details can be found in the SI.

Theory of the intrinsic spectral function. Most first-principles photoemission calculations determine the spectral function of the photohole (i.e., of the material with a missing electron), which is termed the intrinsic spectral function. Our calculation of this ideal intrinsic spectral functions relies on the first-principles GW+C approach described in (20, 21). We first determine matrix elements of the exchange-correlation self-energy $\Sigma^{\ell\ell}_{xc}(\omega)$ in the GW approximation (49) of many-body perturbation theory, using eigenvalue

self-consistency. Matrix elements of the one-body Green's function for occupied states ℓ are then calculated using the time-ordered cumulant expression (20, 21)

$$G_\ell(\tau) = \mathrm{i}\theta(-\tau)e^{-\mathrm{i}\varepsilon_\ell\tau}e^{C_\ell(\tau)}$$
$$C_\ell(\tau) = \frac{1}{\pi}\int_{-\infty}^{E_F-\varepsilon_\ell} \mathrm{d}\omega \left|\mathrm{Im}\Sigma^{\ell\ell}_{xc}(\omega+\varepsilon_\ell)\right| \frac{e^{-\mathrm{i}\omega\tau}-1}{\omega^2}\,, \quad [1]$$

where the QP energy $\varepsilon_\ell < E_F$, with E_F the Fermi energy, is a result of the GW calculation. The imaginary part of the GW self-energy matrix elements reads

$$\mathrm{Im}\Sigma^{\ell\ell}_{xc}(\omega+\varepsilon_\ell) = \sum_{j,s\neq 0} |V^s_{\ell j}|^2 \delta(\omega+\varepsilon_\ell-\varepsilon_j+\omega_s)\,. \quad [2]$$

Here, ω_s are energies of neutral charge excitations such as plasmons and interband transitions, and $|V^s_{\ell j}|$ are matrix elements of the fluctuation potentials (6), determining the strength of the coupling of these excitations to the QP. In an electron-boson coupling picture ω_s are boson energies and $|V^s_{\ell j}|$ the electron-boson coupling strength. The most important contributions are given by the states j that are close to ℓ. Hence, one can understand the satellite shape dispersion from Eq. (2): in the case of Γ, which is at the bottom of a parabolic valence band, no state can contribute to the sum with energy $\varepsilon_j < \varepsilon_\ell$. As a result, as shown in Fig. 3(a), the shape of $\mathrm{Im}\Sigma^{\ell\ell}_{xc}(\omega+\varepsilon_\ell)$ is asymmetric, with a tail towards smaller binding energies. In the case of L, instead, states contributing to the sum can have energies that are either larger or smaller than ε_ℓ, which makes the shape of $\mathrm{Im}\Sigma^{\ell\ell}_{xc}(\omega+\varepsilon_\ell)$ more symmetric. Since the dispersion at L is much steeper than at the bottom of the band, there is also more broadening. This is then directly reflected in the shape of the satellites in the spectral functions shown in Fig. 3(b). The imaginary part of the Fourier transform of G_ℓ in the frequency domain yields the intrinsic spectral function $A_\ell(\omega) = \pi^{-1}|\mathrm{Im}\, G_\ell(\omega)|$. The spectral functions are evaluated along ΓL. Since the experimental paths correspond to small k_z deviations from the ΓL path, we shift calculated energies by 0.2 eV (0.9 eV) in the simulation of the 624 eV (1100 eV) photon energy spectra. These shifts are no fit parameters, but obtained from our first-principles calculation of the band dispersion along k_z.

The calculated spectra are multiplied by a constant factor to match the arbitrary experimental units. For the relative weight of different bands, we start from calculated intensities based on a projection on atomic cross sections (50), but for valence bands of delocalized-electron materials like aluminum, this is not precise enough. We therefore fit the ratio of the cross sections of the two valence bands to the experimental QP ratios. This changes the intensity of the QP at L by about 50 %. Note again that only QP intensities are adjusted, whereas no parameter is used concerning the satellites, which are the topic of the present work. We include Gaussian broadenings to account for the experimental angle and energy resolutions and multiply all the spectra by a Fermi function with a temperature of 50 K. For computational details see the SI.

Inelastic scattering. To include extrinsic and interference effects, following (14) $\mathrm{Im}\,\Sigma_{xc}(\omega+\varepsilon)$ is multiplied by a frequency (ω)- and photon energy (ν)-dependent enhancement factor $R_\nu(\omega)$ derived from the semi-infinite electron gas in (6, 26, 44). For $R_\nu = 1$ the extrinsic and interference terms cancel and the spectra are given by the intrinsic spectral function.

ACKNOWLEDGMENTS. Computation time was granted by GENCI (Project No. 544). This work has received funding from the European Research Council (ERC Grant Agreement n. 320971) and from a Marie Curie FP7 Integration Grant within the 7th European Union Framework Programme. This work was also supported by a public grant overseen by the French National Research Agency (ANR) as part of the "Investissements d'Avenir" program (Labex NanoSaclay, reference: ANR-10-LABX-0035) and by the Labex Palm (Grant No. ANR-10-LABX-0039-PALM). JJR and JJK acknowledge funding support from DOE Office of Science BES Grant No. DE-FG02-97ER45623. We acknowledge the Paul Scherrer Institut, Villigen, Switzerland for synchrotron radiation beamtime at the PEARL beamline of the Swiss Light Source.

1. S Hüfner, *Photoelectron Spectroscopy: Principles and Applications.* (Springer, Berlin), (2003).
2. RM Martin, L Reining, DM Ceperley, *Interacting Electrons.* (Cambridge University Press), (2016).
3. M van Schilfgaarde, T Kotani, S Faleev, Quasiparticle self-consistent gw theory. *Phys. Rev. Lett.* **96**, 226402 (2006).
4. DC Langreth, Singularities in the x-ray spectra of metals. *Phys. Rev. B* **1**, 471–477 (1970).
5. L Hedin, BI Lundqvist, S Lundqvist, Beyond the one-electron approximation: Density of states for inbteracting electrons in *Electronic Density of States*, ed. LH Bennett. (National Bureau of Standards (U.S.), Washington), p. 233 (1971).
6. L Hedin, On correlation effects in electron spectroscopies and the GW approximation. *J. Phys. Condens. Matter* **11**, R489–R528 (1999).
7. F Aryasetiawan, L Hedin, K Karlsson, Multiple plasmon satellites in na and al spectral functions from *Ab Initio* cumulant expansion. *Phys. Rev. Lett.* **77**, 2268–2271 (1996).
8. GD Mahan, *Many Particle Physics, Third Edition.* (Springer, New York), (2000).
9. C Verdi, F Caruso, F Giustino, Origin of the crossover from polarons to fermi liquids in transition metal oxides. *Nat. Commun.* **8**, 15769– (2017).
10. JP Nery, et al., Quasiparticles and phonon satellites in spectral functions of semiconductors and insulators: Cumulants applied to the full first-principles theory and the fröhlich polaron. *Phys. Rev. B* **97**, 115145 (2018).
11. F Bechstedt, *Many-Body Approach to Electronic Excitations: Concepts and Applications.* (Springer), (2014).
12. M Vos, et al., Determination of the energy-momentum densities of aluminium by electron momentum spectroscopy. *J. Physics: Condens. Matter* **11**, 3645 (1999).
13. M Vos, et al., Quantitative measurement of the spectral function of aluminum and lithium by electron momentum spectroscopy. *Phys. Rev. B* **66**, 155414 (2002).
14. M Guzzo, et al., Valence electron photoemission spectrum of semiconductors: *Ab Initio* description of multiple satellites. *Phys. Rev. Lett.* **107**, 166401 (2011).
15. J Lischner, D Vigil-Fowler, SG Louie, Physical origin of satellites in photoemission of doped graphene: An *Ab Initio* gw plus cumulant study. *Phys. Rev. Lett.* **110**, 146801 (2013).
16. AS Kheifets, VA Sashin, M Vos, E Weigold, F Aryasetiawan, Spectral properties of quasiparticles in silicon: A test of many-body theory. *Phys. Rev. B* **68**, 233205 (2003).
17. J Lischner, et al., Satellite band structure in silicon caused by electron-plasmon coupling. *Phys. Rev. B* **91**, 205113 (2015).
18. F Caruso, H Lambert, F Giustino, Band structures of plasmonic polarons. *Phys. Rev. Lett.* **114**, 146404 (2015).
19. JJ Kas, JJ Rehr, L Reining, Cumulant expansion of the retarded one-electron Green function. *Phys. Rev. B* **90**, 085112 (2014).
20. JS Zhou, et al., Dynamical effects in electron spectroscopy. *The J. Chem. Phys.* **143**, 184109 (2015).
21. JS Zhou, M Gatti, JJ Kas, JJ Rehr, L Reining, Cumulant green's function calculations of plasmon satellites in bulk sodium: Influence of screening and the crystal environment. *Phys. Rev. B* **97** (2018).
22. B Gumhalter, V Kovač, F Caruso, H Lambert, F Giustino, On the combined use of gw approximation and cumulant expansion in the calculations of quasiparticle spectra: The paradigm of si valence bands. *Phys. Rev. B* **94**, 035103 (2016).
23. F Caruso, C Verdi, S Poncé, F Giustino, Electron-plasmon and electron-phonon satellites in the angle-resolved photoelectron spectra of n-doped anatase $\mathrm{tio_2}$. *Phys. Rev. B* **97**, 165113 (2018).
24. T Kloos, Plasmaschwingungen in al, mg, li, na und k angeregt durch schnelle elektronen. *Z. Physik A* **265**, 225–238 (1973).
25. M Cazzaniga, et al., Dynamical response function in sodium and aluminum from time-dependent density-functional theory. *Phys. Rev. B* **84**, 075109 (2011).
26. L Hedin, J Michiels, J Inglesfield, Transition from the adiabatic to the sudden limit in core-electron photoemission. *Phys. Rev. B* **58**, 15565–15582 (1998).
27. F Giustino, Electron-phonon interactions from first principles. *Rev. Mod. Phys.* **89**, 015003 (2017).
28. NJ Shevchik, Theory of angle-resolved photoemission from the bulk bands of solids. iii. effects of intra-atomic and interatomic electron-phonon interactions. *Phys. Rev. B* **20**, 3020–3029 (1979).
29. Z Hussain, CS Fadley, S Kono, LF Wagner, Temperature-dependent angle-resolved x-ray photoemission study of the valence bands of single-crystal tungsten: Evidence for direct transitions and phonon effects. *Phys. Rev. B* **22**, 3750–3766 (1980).
30. J Braun, et al., Exploring the xps limit in soft and hard x-ray angle-resolved photoemission using a temperature-dependent one-step theory. *Phys. Rev. B* **88**, 205409 (2013).
31. P Hofmann, et al., Unexpected surface sensitivity at high energies in angle-resolved photoemission. *Phys. Rev. B* **66**, 245422 (2002).
32. AX Gray, et al., Probing bulk electronic structure with hard x-ray angle-resolved photoemission. *Nat. Mater.* **10**, 759– (2011).
33. L Plucinski, et al., Band mapping in higher-energy x-ray photoemission: Phonon effects and comparison to one-step theory. *Phys. Rev. B* **78**, 035108 (2008).
34. C Papp, et al., Band mapping in x-ray photoelectron spectroscopy: An experimental and theoretical study of w(110) with 1.25 kev excitation. *Phys. Rev. B* **84**, 045433 (2011).
35. EW Plummer, Photoemission from nearly free electron metals. *Phys. Scripta* **1987**, 186 (1987).
36. ED Hansen, T Miller, TC Chiang, Surface photoemission in ag(100). *Phys. Rev. B* **55**, 1871–1875 (1997).
37. V Strocov, Intrinsic accuracy in 3-dimensional photoemission band mapping. *J. Electron Spectrosc. Relat. Phenom.* **130**, 65 – 78 (2003).
38. L Hedin, On correlation effects in electron spectroscopies and the gw approximation. *J. Physics: Condens. Matter* **11**, R489 (1999).
39. G Mahan, Electron energy loss during photoemission. *Phys. Status Solidi B* **55**, 703–710 (1973).
40. WJ Pardee, et al., Analysis of surface- and bulk-plasmon contributions to x-ray photoemission

spectra. *Phys. Rev. B* **11**, 3614–3616 (1975).
41. CN Berglund, WE Spicer, Photoemission studies of copper and silver: Theory. *Phys. Rev.* **136**, A1030–A1044 (1964).
42. PM Th., M van Attekum, JM Trooster, Bulk- and surface-plasmon-loss intensities in photo-electron, auger, and electron-energy-loss spectra of al metal. *Phys. Rev. B* **18**, 3872–3883 (1978).
43. S Tougaard, P Sigmund, Influence of elastic and inelastic scattering on energy spectra of electrons emitted from solids. *Phys. Rev. B* **25**, 4452–4466 (1982).
44. W Bardyszewski, L Hedin, A new approach to the theory of photoemission from solids. *Phys. Scripta* **32**, 439 (1985).
45. HJ Levinson, F Greuter, EW Plummer, Experimental band structure of aluminum. *Phys. Rev. B* **27**, 727–747 (1983).
46. M Muntwiler, et al., Surface science at the pearl beamline of the swiss light source. *J. Synchrotron Radiat.* **24**, 354–366 (2017).
47. CS Fadley, Photoelectron diffraction. *Phys. Scripta* **T17**, 39–49 (1987).
48. MAV Alvarez, H Ascolani, G Zampieri, Excitation of phonons and forward focusing in x-ray photoemission from the valence band. *Phys. Rev. B* **54**, 14703–14712 (1996).
49. L Hedin, New method for calculating the one-particle green's function with application to the electron-gas problem. *Phys. Rev.* **139**, A796–A823 (1965).
50. J Yeh, I Lindau, Atomic subshell photoionization cross sections and asymmetry parameters: 1 le z le 103. *At. Data Nucl. Data Tables* **32**, 1 – 155 (1985).